more when considering particular patterns of increased uptake that are frequently caused by sterile inflammatory processes (e.g., uptake around the neck of a total hip prosthesis or uptake in the synovial lining only).

ACKNOWLEDGMENTS

We thank Mr. Antoi Meeuwis and his staff and Mr. Emile Koenders for their help in performing the study.

REFERENCES

1. Wegener WA, Alavi A. Diagnostic imaging of muskuloskeletal infection. Roentgenography; gallium, indium-labeled white blood cell, gammaglobulin, bone scintigraphy; and MRI. *Orthop Clin North Am* 1991;22:401–418.
2. Elgazzar AH, Abdel-Dayem HM, Clark JD, Maxon HR. Multimodality imaging of osteomyelitis. *Eur J Nucl Med* 1995;22:1043–1063.
3. Palestro CJ. The current role of gallium imaging in infection. *Semin Nucl Med* 1994;24:128–141.
4. Palestro CJ, Kim CK, Swyer AJ, Capozzi JD, Solomon RW, Goldsmith SJ. Total-hip arthroplasty: periprosthetic indium-111-labeled leukocyte activity and complementary technetium-99m-sulfur colloid imaging in suspected infection. *J Nucl Med* 1990;31: 1950–1955.
5. Schauwecker DS. Osteomyelitis: diagnosis with In-111-labeled leukocytes. *Radiology* 1989;171:141–146.
6. Rubin RH, Fischman AJ. The use of radiolabeled nonspecific immunoglobulin in the detection of focal inflammation. *Semin Nucl Med* 1994;14:1110–1118.
7. Rubin RH, Fischman AJ, Callahan RJ, et al. In-111-labeled nonspecific immunoglobulin scanning in the detection of focal infection. *N Engl J Med* 1989;321:935–940.
8. Oyen WJG, Claessens RAMJ, van der Meer JWM, Rubin RH, Strauss HW, Corstens FHM. Indium-111-labeled human nonspecific immunoglobulin G: a new radiopharmaceutical for imaging infectious and inflammatory foci. *Clin Infect Dis* 1992;14:1110–1118.
9. Oyen WJG, Claessens RAMJ, van Horn JR, van der Meer JWM, Corstens FHM. Scintigraphic detection of bone and joint infections with indium-111-labeled nonspecific polyclonal human immunoglobulin G. *J Nucl Med* 1990;31:403–412.
10. Oyen WJG, van Horn JR, Claessens RAMJ, Slooff TJJH, van der Meer JWM, Corstens FHM. Diagnosis of bone, joint and joint prosthesis infections with indium-111-labeled nonspecific human immunoglobulin G scintigraphy. *Radiology* 1992;182:195–199.
11. Oswald SG, van Nostrand D, Savory CG, Callaghan JJ. Three-phase bone and indium white blood cell scintigraphy following porous-coated hip arthroplasty. *J Nucl Med* 1990;30:274–280.
12. Rosenthall L, Lepanto L, Raymond F. Radiophosphate uptake in asymptomatic knee arthroplasty. *J Nucl Med* 1987;28:1546–1549.
13. Palestro CJ, Swyer AJ, Kim SK, Goldsmith SJ. Infected knee prosthesis: diagnosis with In-111 leukocyte, Tc-99m sulfur colloid and Tc-99m MDP imaging. *Radiology* 1991;179:645–648.
14. Datz FL. Indium-111-labeled leukocytes for the detection of infection: current status. *Semin Nucl Med* 1994;24:169–179.
15. Ezuddin S, Yuille D, Spiegelhoff D. The role of dual bone and WBC scan imaging in the evaluation of osteomyelitis and cellulitis using both planar and SPECT imaging. *J Nucl Med* 1992;33:839.
16. Yuh WTC, Corson JD, Baraniewsky HM, et al. Osteomyelitis of the foot in diabetic patients: evaluation with plain film, Tc-99m bone scintigraphy and MR imaging. *Am J Roentgenol* 1989;152:795–800.
17. Keenan AM, Tindel NL, Alavi A. Diagnosis of pedal osteomyelitis in diabetic patients using current scintigraphic techniques. *Arch Intern Med* 1989;149:2262–2266.
18. Larcos G, Brown ML, Sutton RT. Diagnosis of osteomyelitis of the foot in diabetic patients: value of In-111 leukocyte scintigraphy. *Am J Roentgenol* 1991;157:527–531.
19. Kolindou A, Liu Y, Ozker K, et al. Indium-111 WBC imaging of osteomyelitis in patients with underlying bone scan abnormalities. *Clin Nucl Med* 1996;21:183–191.
20. Oyen WJG, Netten PM, Lemmens JA, et al. Evaluation of infectious diabetic foot complications with indium-111-labeled human nonspecific immunoglobulin G. *J Nucl Med* 1992;33:1330–1336.
21. Nepola JV, Seabold JE, Marsh JL, Kirchner PT, El-Khoury GY. Diagnosis of infection in ununited fractures: combined imaging with indium-111-labeled leukocytes and technetium-99m methylene diphosphonate. *J Bone Jt Surg Am Vol* 1993;75:1816–1822.
22. de Bois MHW, Pauwels EKJ, Breedveld FC. New agents for scintigraphy in rheumatoid arthritis. *Eur J Nucl Med* 1995;22:1339–1346.
23. Oyen WJG, Claessens RAMJ, Raemaekers JMM, de Pauw BE, van der Meer JWM, Corstens FHM. Diagnosing infection in febrile granulocytopenic patients with indium-111-labeled human IgG. *J Clin Oncol* 1992;10:61–68.
24. Datz FL, Morton KA. Radionuclide detection of occult infection: current strategies. *Cancer Invest* 1991;9:691–698.
25. Whalen JL, Brown ML, McLeod R, et al. Limitations of indium leukocyte imaging for the diagnosis of spine infections. *Spine* 1991;16:193–197.26.
26. Palestro CJ, Kim CK, Swyer AJ, Vallabhajosula, Goldsmith SJ. Radionuclide diagnosis of vertebral osteomyelitis: indium-111-leukocyte and technetium-99m-methylene diphosphonate bone scintigraphy. *J Nucl Med* 1991;32:1861–1865.
27. Sciuk J, Brandau W, Vollet B, et al. Comparison of technetium-99m polyclonal human immunoglobulin and technetium-99m monoclonal antibodies for imaging chronic osteomyelitis: first clinical results. *Eur J Nucl Med* 1991;8:401–407.
28. Goh ASW, Aw SE, Sundram FX, Ang ES, Goh SK, Leong KH. Imaging of focal inflammation with ^{99m}Tc-labeled human polyclonal immunoglobulin G. *Nucl Med Commun* 1990;11:843–856.
29. Modic M, Feiglin DH, Piraino DW, et al. Vertebral osteomyelitis: assessment using MR. *Radiology* 1985;157:157–166.
30. Unger E, Moldofsky P, Gatenby R, Hartz W, Broder G. Diagnosing osteomyelitis by MR imaging. *Am J Roentgenol* 1988;150:605–610.
31. Totty WG. Radiographic evaluation of osteomyelitis using magnetic resonance imaging. *Orthop Rev* 1989;18:587–592.

Imaging of the Pancreas and Related Diseases with PET Carbon-11-Acetate

Paul D. Shreve and Milton D. Gross

Department of Nuclear Medicine, Ann Arbor Veterans Affairs Medical Center and Department of Internal Medicine, Division of Nuclear Medicine, University of Michigan Medical Center, Ann Arbor, Michigan

The purpose of this study was to evaluate [1-^{11}C]-acetate as a tracer for functional imaging of the pancreas and related diseases using positron emission tomography (PET). **Methods:** Thirty-three patients underwent 30 min of dynamic attenuation-corrected PET after intravenous administration of 740 MBq (20 mCi) of [1-^{11}C]-acetate. **Results:** The normal pancreas demonstrates prompt uptake of [1-^{11}C]-acetate and is visualized as early as 2 min post-injection, with maximal activity achieved by 5 min. Subsequent clearance of tracer from the pancreas is slow relative to adjacent organs and background, such that by 10 min post-injection the pancreas is the most prominent organ in the imaging field of view. Pancreatic uptake of [1-^{11}C]-acetate was unaffected by pancreatic endocrine insufficiency, but is absent in chronic pancreatitis complicated by exocrine insufficiency. Moderately reduced [1-^{11}C]-acetate uptake was observed in acute uncomplicated pancreatitis. The level of tracer accumulation was substantially reduced in phlegmatous masses complicating pancreatitis and in chronic mass forming pancreatitis. Adenocarcinoma of the pancreas likewise demonstrated no significant uptake of [1-^{11}C]-acetate. **Conclusions:** Accumulation of [1-^{11}C]-acetate by the pancreas allows rapid metabolic imaging using PET, and may be a useful metabolic probe for the study of pancreatic physiology and disease.

Key Words: pancreas; PET; acetate; neoplasm; pancreatitis

J Nucl Med 1997; 38:1305–1310

Imaging diagnosis of pancreatic disease has been primarily based on descriptions of anatomic pathology. Despite improvements in cross-sectional structural imaging, many important pancreatic diseases remain inadequately characterized by anatomic criteria alone. For example, the severity of acute pancreatitis can only be inferred by nonspecific morphologic alterations in the pancreas itself and in adjacent tissues, attendant to

Received Apr. 26, 1996; revision accepted Oct. 30, 1996.

For correspondence or reprints contact: Paul D. Shreve, MD, Division of Nuclear Medicine, University of Michigan Medical Center, 1500 E. Medical Center Drive, Box 0028, Ann Arbor, MI 48109-0028.

the appearance of complications such as the formation of inflammatory masses, pancreatic necrosis and parapancreatic fluid collections (*1*). In mild to moderate chronic pancreatitis, the severity of the morphologic abnormality of the gland or duct structures does not correlate with exocrine dysfunction (*2*). A discrete pancreatic mass, when identified, can be a nonspecific finding with respect to cancer without corroborative evidence of malignancy (*3–5*).

Images that depict tissue physiology rather than anatomy would thus be particularly useful in the study of pancreatic physiology and disease. The first functional imaging agent of the pancreas, ^{75}Se-selenomethionine, was described by Blau and Bender in 1962 (*6*). Specificity for both identification of masses and imaging diagnosis of impaired pancreatic exocrine function was low, however, due in part to the limited spatial and temporal resolution (*7*). Furthermore, ^{75}Se-selenomethionine is subject to metabolic pathways independent of L-methionine (*8*). L-methionine labeled with ^{11}C is a true tracer of the amino acid and follows the pathway of active transport into the acinar pancreas cells with subsequent incorporation into the pancreatic zymogens. When imaged with positron emission tomography (PET), ^{11}C-L-methionine allows for substantially improved spatial and temporal resolution over the single photon agent ^{75}Se-selenomethionine (*9*). Absence of functioning acinar tissue due to the presence of a space occupying mass or chronic pancreatitis could be identified on images by the absence of ^{11}C-L-methionine tracer uptake (*9,10*). Additionally, by duodenal intubation and aspiration, subsequent secretion of the labeled protein into excreted pancreatic juices under secretagogue stimulation has been used as an index of pancreatic exocrine function (*11*).

Both L-methionine tracers are limited by the pathway of amino acid carrier-mediated uptake and incorporation into exocrine proteins, a process resulting in prolonged tracer kinetics. A tracer capable of similar high pancreas target-to-background ratios but with more rapid uptake and clearance reflecting a more central aspect of pancreatic tissue metabolism may provide greater versatility and applicability in the study of pancreatic function and disease, or serve a complimentary role to other functional tracers for pancreas imaging.

As a probe of intermediary metabolism, [1-^{11}C]-acetate has been widely investigated for the study myocardial metabolism (*12–15*). The behavior of this tracer elsewhere, particularly the visceral organs, to date has received little attention. In vitro studies over 2 decades ago using [1-^{14}C]-acetate and rat pancreatic fragments demonstrated highly active basal lipid metabolism with rapid incorporation of [1-^{14}C]-acetate into fatty acids (*16*). In our recent studies of [1-^{11}C]-acetate behavior in the kidney (*17*), we observed remarkably high uptake and retention of [1-^{11}C]-acetate tracer activity in the pancreas relative to other visceral organs, suggesting the earlier in vitro observations of pancreas acetate metabolism apply to in vivo imaging applications. We describe here our initial findings concerning the use of [1-^{11}C]-acetate as a functional imaging agent for the pancreas and related diseases.

MATERIALS AND METHODS

Patients

After institutional human use committee approval, 33 patients from the Ann Arbor Veterans Affairs Hospital were studied. All patients gave written informed consent. Twelve patients with no history of pancreatic related disease, or laboratory or clinical findings to indicate pancreatic disease ranging in age from 24 to 69 yr were used as normal controls. Six patients with a long standing history of insulin-requiring diabetes mellitus and five patients with a long standing history of chronic pancreatitis complicated by clinical signs and symptoms of exocrine insufficiency were studied to assess the effect of pancreatic endocrine and exocrine insufficiency, respectively, on pancreas uptake and retention of [1-^{11}C]-acetate. Three patients were studied during episodes of acute uncomplicated pancreatitis, with serum amylase and lipase levels in excess of 500 international units/liter and 200 international units/dl, respectively, at the time of scanning. Three patients with inflammatory pancreatic masses were also studied; one patient with chronic mass forming pancreatitis and two with active phlegmatous masses. Additionally, five patients with pancreatic adenocarcinoma, one adenocystic, were studied. Diagnosis of the pancreatic masses was by histopathology, except for one case of phlegmatous masses for which diagnosis was confirmed by 2-yr clinical and serial computed tomography (CT) scan follow-up.

Radiotracer Preparation

Carbon-11 was produced using a CS-30 cyclotron by proton bombardment of $^{14}N_2$. The resultant $^{11}CO_2$ was then reacted with methyl magnesium bromide by a modified method of Pike et al. (*18*). Radionuclide purity of the [1-^{11}C]-acetate was greater than 98% and radiochemical purity determined by radio high pressure liquid radiochromatography was consistently greater than 95%.

Imaging Protocol

Patients underwent dynamic PET using a Siemens ECAT 931 or ECAT Exact 921 scanner. All patients studied fasted 6–12 hr before scanning to minimize variability in substrate availability due to meals and to preclude bowel uptake of tracer (which we had observed incidentally in past [1-^{11}C]-acetate studies of patients who had inadvertently eaten before scanning). Serum glucose in all patients was between 80 and 150 mg/dl at time of scanning. Patients were positioned in the scanner gantry such that the pancreas was centered in the axial field of the scanner based on the relationship of the pancreas so such landmarks as the xiphoid, umbilicus and iliac crests on CT. A 15-min transmission scan using a ^{68}Ge ring source (931 scanner) or ^{68}Ge retractable rod source (ECAT Exact 921 scanner) was performed for attenuation correction purposes before tracer administration. Carbon-11-acetate [740 MBq (20 mCi)] in normal saline was then administered intravenously over 30 sec using a calibrated dose injector, with simultaneous initiation of 30 min of dynamic emission imaging. The image sequence included ten 10-sec imaging frame acquisitions followed by ten 20-sec frames, two 2.5-min frames and four 5-min frames.

Image and Data Analysis

Attenuation- and decay-corrected images were reconstructed transaxially and displayed in a 128 × 128 matrix. Images were visually evaluated using a computer display of the transaxial reconstructions of image frames from 10–20 min, as well as the entire dynamic sequence at selected axial levels. In all patients except normal controls, correlative CT scans were available for comparison to aid in locating focal pathologies, which were not tracer avid. To examine tissue tracer time-activity relationships, two regions of interest (ROIs) were drawn, one predominantly in the pancreas head, the other centered in the body and tail of the gland. These ROIs ranged in size from 12–40 pixels (pixel size 4.7 and 4.2 mm for the 931 and 921 model scanners, respectively). Additional regions of interest were drawn for masses or focal areas of inflammation in those subjects with such pathologies, as well as regions of liver and renal cortex included in the field of view. ROIs were drawn well within the tissue tracer activity to minimize partial volume averaging error. Tracer activity was then expressed as

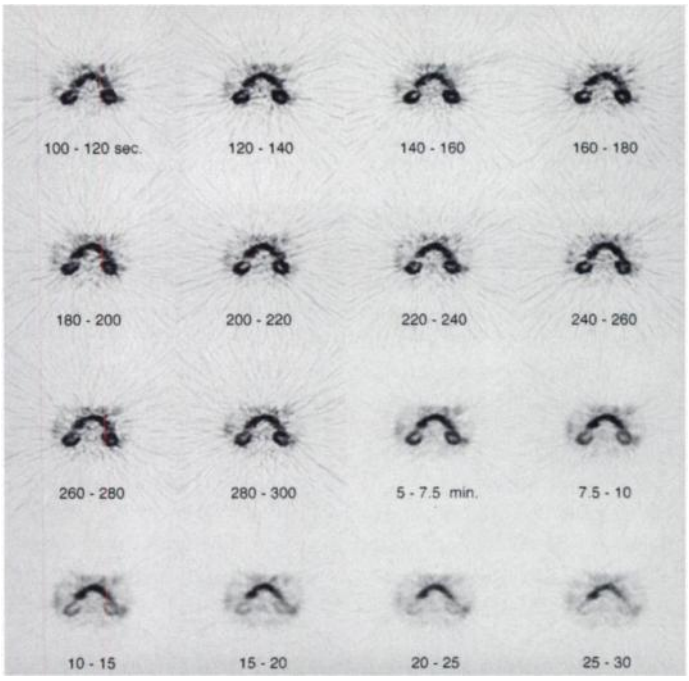

FIGURE 1. Sequential decay- and attenuation-corrected transaxial images of the pancreas after intravenous administration of 740 MBq (20 mCi) of [1-^{11}C]-acetate. Image frame times are post-tracer administration.

average counts per pixel for the ROI normalized to 1 cm^3 voxel volume.

ROI tracer activity was additionally expressed as standardized uptake value (SUV) using the following relationship: SUV equals average recorded counts per pixel × patient weight (kg)/scanner calibration factor × administered dose (mCi). For comparison of tissue tracer activity among normal pancreas and various pathologies, the SUV at 10–20 min post-tracer administration ($SUV_{10-20\ min}$) was chosen as optimal target-to-nontarget ratio was achieved beyond 10 min and changed little thereafter. Differences in the $SUV_{10-20\ min}$ values of normal control subjects, endocrine and exocrine insufficient categories were tested for statistical significance using unpaired Student's t-test, after homogeneity of variance between the $SUV_{10-20\ min}$ values of the categories was confirmed by the Bartlett's test.

RESULTS

Images of the Pancreas

Uptake of [1-^{11}C]-acetate by pancreatic tissue is rapid, with the organ clearly visualized by 2 min (Fig. 1). Tracer continues to accumulate in the pancreas relative to adjacent organs and background, such that by 10 min the pancreas is the most prominent organ in the imaging field. By 30 min post-injection, the pancreas remains well-defined and is the only remaining conspicuous structure in the imaging field. The head, body and tail of the pancreas are well-delineated on images beyond 10 min due to the high target-to-background ratio. The pancreas-to-liver ratio 10–20 min post-injection ranged from 2.1–4.5, with a mean of 3.1, among the normal subjects studied.

Pancreatic uptake of [1-^{11}C]-acetate in subjects with greater than 10 yr of insulin-requiring diabetes mellitus was not visually altered (Fig. 2), nor was uptake and retention of tracer as measured by $SUV_{10-20\ min}$ significantly different from patients with normal pancreatic endocrine function (Fig. 3). Patients with chronic pancreatitis complicated by exocrine insufficiency, however, demonstrated no discernible accumulation of tracer above background in the pancreatic bed (Fig. 2) and the $SUV_{10-20\ min}$ was significantly ($p < 0.001$) less than normal controls and diabetic patients (Fig. 3). Moderately

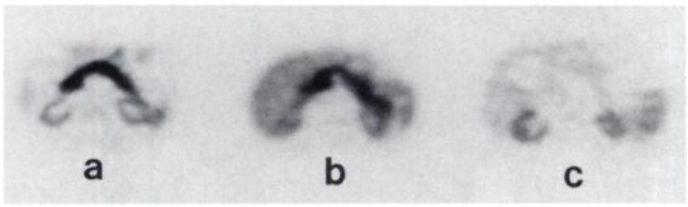

FIGURE 2. Transaxial [1-^{11}C]-acetate images at the level of the pancreas 10–20 min after tracer administration. (a) Normal patient. (b) Patient with long-standing insulin-requiring diabetes mellitus. (c) Patient with chronic alcoholic pancreatitis complicated by exocrine insufficiency. Images are attenuation and decay corrected.

reduced uptake of [1-^{11}C]-acetate was observed in the pancreas of patients with acute uncomplicated pancreatitis (Fig. 3).

Inflammatory masses including phlegmatous masses and a pseudomass of chronic pancreatitis did not accumulate [1-^{11}C]-acetate (Fig. 3). Masses due to pancreatic adenocarcinoma likewise did not accumulate [1-^{11}C]-acetate (Fig. 3). Such non-[1-^{11}C]-acetate avid masses could be typically identified, however, by distortion or displacement of [1-^{11}C]-acetate avid uninvolved pancreas tissue. For example, as shown in Figure 4, an adenocarcinoma in the head of the pancreas is clearly identified by a hole of absent tracer activity surrounded by acetate avid nonneoplastic pancreatic tissues. Similarly, in another patient, a neoplastic mass is identified by effacement of the anterolateral aspect of the pancreatic head. Absent sustained uptake of tracer in a case of chronic mass-forming pancreatitis originating in the posterior aspect of the pancreatic tail is revealed by anterior displacement and draping of the noninvolved pancreatic tail is over the mass. In another patient shown in Figure 4, a phlegmatous mass is displacing the uninvolved pancreatic head laterally.

No significant bowel uptake of the tracer was present in fasted patients. Subjects who inadvertently ate before scanning demonstrated intense small bowel uptake of tracer, which was readily apparent throughout the small bowel on the earliest imaging frames indicating that the tracer uptake was due to direct extraction from blood rather than excretion of tracer contained in pancreatic secretions. Intense renal uptake was seen in all the subjects that cleared rapidly, concordant with our

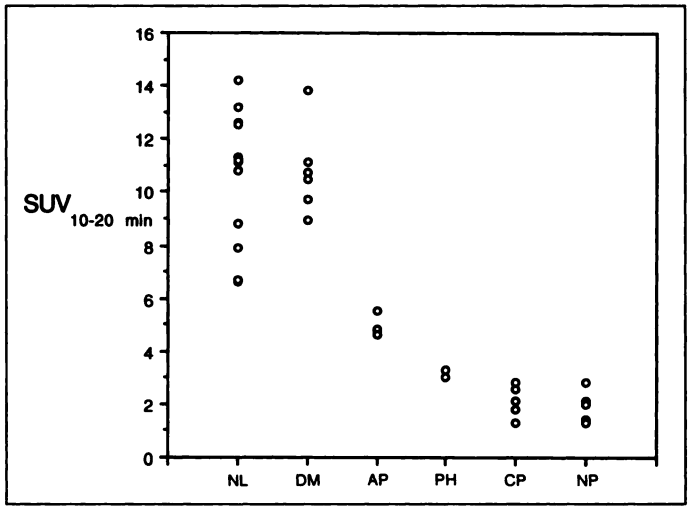

FIGURE 3. Comparison of standardized uptake values of tissue tracer activity in the pancreas at 10–20 min post-[1-^{11}C]-acetate administration ($SUV_{10-20\ min}$) in normal patients (NL), insulin requiring diabetes mellitus (DM), acute uncomplicated pancreatitis (AP), and in the pancreatic bed of patients with chronic pancreatitis with exocrine insufficiency (CP). Also shown are ($SUV_{10-20\ min}$) of pancreatic masses including phlegmon (PH) and pancreatic adenocarcinoma (NP).

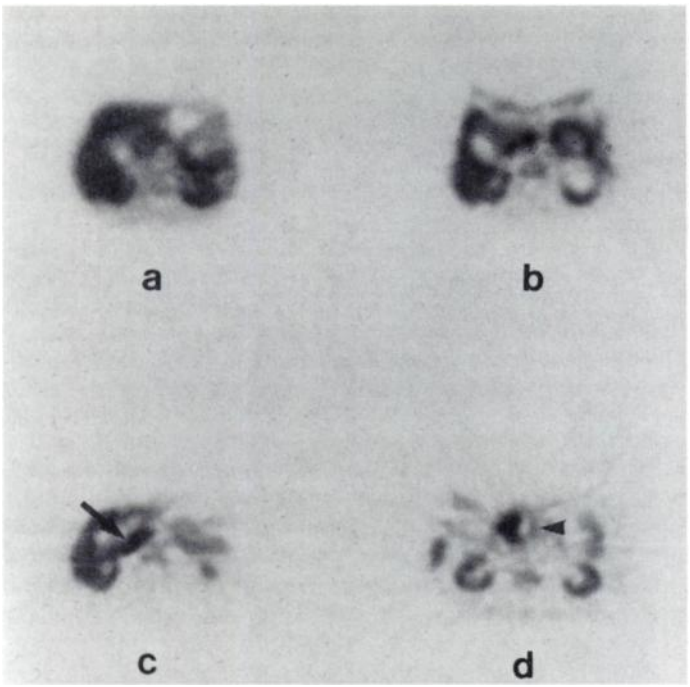

FIGURE 4. Transaxial [1-^{11}C]-acetate images at the level of the pancreas 10–20 min post-tracer administration in patients with pancreatic masses. (a) Adenocarcinoma in the head of the pancreas. Acetate avid normal pancreatic tissue is distorted around the neoplasm. The neoplasm itself is seen as a relative photopenic defect in the pancreatic head because it shows no appreciable uptake of [1-^{11}C]-acetate. (b) Chronic mass forming pancreatitis in the posterior tail of the pancreas. The uninvolved pancreas tissue is displaced anteriorly and draped over the mass, which itself shows only low level uptake of [1-^{11}C]-acetate. (c) Neoplastic mass at the anterolateral margin of the head of the pancreas, causing effacement and displacement of the nonneoplastic pancreas tissue of the pancreatic head (arrow). (d) Phlegmatous mass displacing the pancreatic head laterally (arrowhead). Uninvolved pancreas tissue shows normal tracer uptake.

previously described findings (*17*). The liver was generally associated with modest [1-^{11}C]-acetate uptake, but in a few patients tracer uptake was relatively intense, approaching nearly one-half the intensity of pancreas tissue. In all cases, however, the pancreas was readily distinguishable from the liver.

Tissue Time-Activity Curves

The pancreas rapidly accumulated [1-^{11}C]-acetate, with peak activity reached by roughly 5 min (Fig. 5). Among normal subjects, the time-to-peak pancreas tracer activity ranged from 3–7.5 min with a mean of 4.6 min and s.d. of 1.1 min.

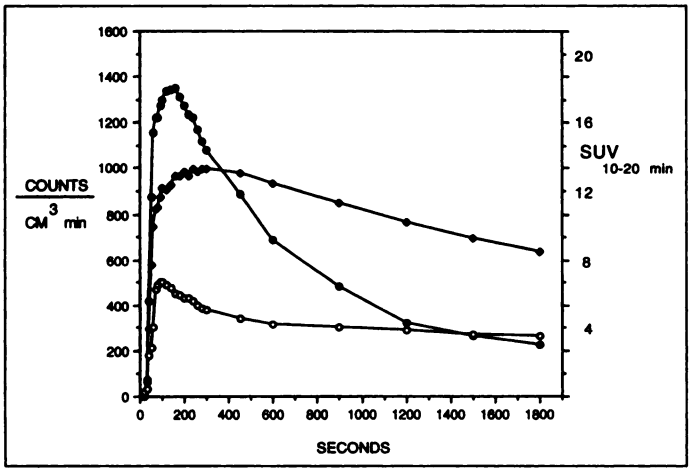

FIGURE 5. Tissue time-activity of [1-^{11}C]-acetate for normal pancreas (◆), normal kidney (●), and normal liver (○). All curves are decay corrected.

Thereafter, clearance of tracer activity was slow, with only about one-third of peak activity lost by 30 min. Among normal subjects, the percent of peak pancreas tracer activity remaining at 30 min ranged from 52% to 75%, with a mean of 64% and s.d. of 6.5%. This is in contrast to tracer activity in the renal cortex, which although it achieved slightly earlier attainment of peak tracer activity, was consistently characterized by much more rapid subsequent clearance of ^{11}C tracer activity. The time-activity of liver also shown in Figure 5 was characterized by slow clearance of tracer activity, somewhat similar to pancreas time-activity, but at a much lower overall level of uptake. The initial rise and falloff of liver tracer activity in the first 3 min of the time-activity curve was usually present but never substantial.

DISCUSSION

Functional imaging agents for the pancreas were anticipated by Josef Rösch three decades ago (*19*) as a means of approaching what was then considered a radiologically hidden organ. Until now, the only physiologic imaging agent available for pancreas imaging has been labeled amino acids, chiefly ^{75}Se- or ^{11}C-labeled L-methionine. Carbon-11-acetate represents a new physiologic tracer for the pancreas, one with a metabolic pathway related to intermediary metabolism, distinct from amino acid metabolism pathway delivered by L-methionine-based tracers.

PET studies of intermediary metabolism using [1-^{11}C]-acetate have been limited to myocardial oxidative metabolism. We recently reported that the uptake and clearance of [1-^{11}C]-acetate by renal parenchyma was similar to that of myocardium (*17*), concordant with the high blood flow and intense oxidative metabolism associated with the renal cortex. Substantial uptake of [1-^{11}C]-acetate, but with quite different overall subsequent clearance as compared with myocardium or renal parenchyma, occurs in the pancreas, a finding of potential utility in the study of pancreatic physiology and disease.

The substantial retention of tracer activity beyond 10 min by pancreatic tissue suggests that the ^{11}C of [1-^{11}C]-acetate is actively incorporated into a molecular form of relative stability rather than predominantly and rapidly converted to $^{11}CO_2$, as in the heart or kidney. This relatively stable form of the ^{11}C of [1-^{11}C]-acetate is most likely in acinar tissues, which comprise 85% of the human pancreas (*20*), rather than trapping of endogenously generated $^{11}CO_2$ to $H^{11}CO_3^-$ by the pancreatic tubular cells. For example, acetazolamide (Diamox) had no effect on the degree of [1-^{11}C]-acetate uptake by the pancreas or the time-activity curves (data not shown). Acinar cells are characterized by prodigious production of digestive proteins and packaging of these zymogens in the endoplasmic reticulum for subsequent secretion. The ^{11}C of [1-^{11}C]-acetate could, after incorporation into the citric acid cycle, be routed to amino acids derived from citric acid intermediates and incorporated into zymogens. Alternatively, acetyl-CoA can follow the acetyl-CoA carboxylase pathway to lipid biosynthesis. Given the highly active basal lipid metabolism associated with zymogen granule membrane turnover and the importance of lipid metabolism as a respiratory fuel in pancreas acinar tissue as demonstrated in in vitro studies of rat pancreas fragments (*16*), [1-^{11}C]-acetate may principally be a probe of this anabolic pathway of intermediary metabolism in the pancreas.

Compared with [1-^{11}C]-acetate, the time-activity of L-methionine-based tracers in the pancreas is prolonged, with peak tissue tracer activity reached in 15–20 min and little subsequent clearance, reflecting carrier-mediated amino acid transport into acinar cells and subsequent incorporation into exocrine proteins

(*21,22*). Clearance of ^{11}C-L-methionine is then limited predominantly to excretion of the formed proteins on stimulation (*10*). In contrast, attainment of peak tracer activity in the pancreas is comparatively prompt with [1-^{11}C]-acetate occurring within 5 min. Subsequently, slow, but measurable clearance of tracer is observed. It is doubtful that this loss of tissue tracer activity is in the pancreatic juices, since pancreatic juice flow is minimal in the fasted state, and in any case, no substantial accumulation of tracer was observed in the duodenum on later imaging frames in any of the subjects we studied. The considerably faster clearance of [1-^{11}C]-acetate from pancreas relative to the methionine tracers underscores the different metabolic pathways available to [1-^{11}C]-acetate, which, as a tracer of intermediary metabolism, can undergo direct catabolism to $^{11}CO_2$ in the citric acid cycle or after deposition in fatty acid pools. A much lower level of oxidative metabolism in pancreas tissue relative to myocardium or renal cortex could account for the slower clearance of tissue tracer activity from the pancreas relative to the heart or kidney.

Anatomic delineation of the pancreas on the [1-^{11}C]-acetate images is very good due to the high intrinsic tracer uptake and the absence of significant adjacent background tracer activity bowel and liver tracer activity. The pancreas-to-liver ratios at 10–20 min post-tracer administration averaged slightly over 3:1, with a range of 2.1–4.5 in normal subjects. These ratios are comparable to that reported for ^{75}Se-selenomethionine in human subjects (*23*) or ^{11}C-L-methionine observed in mice (*22*). The variation in the pancreas-to-liver ratios in part reflected variability of liver uptake of [1-^{11}C]-acetate, where $SUV_{10-20\ min}$ ranged from 2.5–6.1 in normal subjects. Even fairly elevated persistent hepatic tracer activity did not interfere with delineation of the pancreas in the patients included in this study, in part due to the high level of tracer activity in the pancreatic tissue, but also the presence of intra-abdominal fat in the middle-aged and elderly patients studied. In patients with little intra-abdominal fat and elevated hepatic tracer uptake, the delineation of pancreas, particularly the pancreatic head, could be less clear. The etiology of the variability of hepatic uptake requires further investigation and may itself provide useful in the study of hepatic metabolism.

As with the L-methionine-based tracers, space-occupying masses could be delineated by distortion or displacement of the uninvolved tracer-avid pancreatic tissue by a nontracer avid neoplasm. Pancreatic adenocarcinoma showed little avidity for [1-^{11}C]-acetate, with uptake approaching that of background activity, suggesting the operative pathways responsible for accumulation of the ^{11}C tracer by pancreas tissue are lost on transformation. Chronic inflammatory masses, including the pseudomass of chronic pancreatitis and phlegmatous masses, also showed no sustained avidity for [1-^{11}C]-acetate above background, consistent with the loss of functional pancreas tissue to scar or inflammatory digestion, respectively. Unlike the reported absence of L-methionine uptake during acute pancreatitis (*9*), we observed only a moderate decrease of [1-^{11}C]-acetate uptake throughout the pancreas in three cases of acute uncomplicated pancreatitis. A larger series of patients with acute pancreatitis, including a range of severity, will be needed to fully assess whether [1-^{11}C]-acetate can serve a marker of inflamed but nonnecrotic pancreas tissue.

As with the L-methionine tracers, the state of the endocrine pancreas did not influence [1-^{11}C]-acetate uptake, consistent with the small mass of islet cells relative to the exocrine component of the pancreas. We observed little or no [1-^{11}C]-acetate uptake in the pancreatic bed of patients with exocrine insufficiency, concordant with observations reported for L-methionine tracers (*9,11*). Early attempts using pancreatic uptake of ^{75}Se-selenomethionine as an index of exocrine pancreatic functional reserve were limited by the image quality and nonquantitative assessment (*24*). More quantitative measures of pancreatic accumulation of ^{11}C-L-methionine using PET did correlate with pancreatic exocrine insufficiency, but some discrepancies were found, possibly related to amino acid back diffusion and disassociation of methionine transport and zymogen incorporation (*10*). The more rapid uptake of [1-^{11}C]-acetate and different metabolic pathway relative to ^{11}C-L-methionine suggests that [1-^{11}C]-acetate could serve as an alternative tracer for a noninvasive imaging method of quantifying pancreatic exocrine functional mass.

Although not a specific tracer for pancreatic tissue, 2-[fluorine-18]-2-deoxy-*D*-glucose (FDG) can be use to identify pancreatic neoplasms due to the generalized increased accumulation of this tracer in neoplasms (*25–29*). Specificity of FDG however can be limited by the elevated FDG uptake associated with inflammation, specifically with respect to diagnosis of a pancreatic mass due to *acute* mass-forming pancreatitis (*26*). Delineating normal and diseased pancreas tissues by their characteristic metabolism of [1-^{11}C]-acetate may be of value as a complement of the metabolic abnormalities revealed with FDG, particularly with respect to distinguishing inflammation from neoplasm and functioning exocrine pancreas from scar tissue of chronic pancreatitis, and warrants further investigation.

CONCLUSION

We have demonstrated that [1-^{11}C]-acetate is a potentially useful tracer for PET studies of the pancreas and related diseases. Maximal tracer activity and optimal target-to-nontarget activity is achieved rapidly, within 10 min of tracer injection. The metabolic pathway of [1-^{11}C]-acetate appears to be distinct from that of the L-methionine tracers, and thus this tracer may provide a new tool for the study and diagnosis of pancreatic diseases. PET studies using [1-^{11}C]-acetate warrant further investigation in the abdominal organs, where this tracer may have utility as a probe of intermediary metabolism.

ACKNOWLEDGMENTS

We thank J. Rothley, T. Hauser, E. McKenna and A. Weeden of the University of Michigan PET Center for their technical assistance and M. Kilbourn, S. Connor, J. Stayanoff and L. Tluczek of the University of Michigan Cyclotron/Radiochemistry laboratory for the [1-^{11}C]-acetate synthesis. This work was supported by the Ann Arbor Veterans Affairs Medical Center.

REFERENCES

1. Buchler M, Malfertheiner P, Beger HG. Correlation of imaging procedures, biochemical parameters, and clinical stage in acute pancreatitis. In: Malfertheiner P, Ditschuneit H, eds. *Diagnostic procedures in pancreatic disease.* Berlin: Springer-Verlag; 1986:123–129.
2. Malfertheiner P, Buchler M. Correlation of imaging and function in chronic pancreatitis. *Radiol Clin North Am* 1989;27:51–64.
3. Neff CC, Simeone JF, Wittenberg J, Mueller PR, Ferrucci JT. Inflammatory pancreatic masses. *Radiology* 1984;150:35–38.
4. Lammer J, Herlinger H, Zalaudek G, Hofler H. Pseudotumorous pancreatitis. *Gastrointest Radiol* 1985;10:59–67.
5. DelMaschio A, Vanzulli A, Sironi S, et al. Pancreatic cancer versus chronic pancreatitis: diagnosis with CA 19–9 assessment, US, CT, and CT-guided fine-needle biopsy. *Radiology* 1991;178:95–99.
6. Blau M, Bender MA. Se^{75} selenomethionine for visualization of the pancreas by isotope scanning [Abstract]. *Radiology* 1962;78:974.
7. Agnew JE, Youngs GR, Lydford R, et al. The false-positive pancreas scan: does it reflect "low-normal" pancreatic function? *J Nucl Med* 1973;15:90–93.
8. Holland JF, Peters S, Bryant B, Blau M. Independence of selenomethionine pathways from those of methionine in mammalian protein metabolism [Abstract]. *J Clin Invest* 1966;45:1024.
9. Syrota A, Comar D, Cerf M, Plummer D, Maziere M, Kellershohn C. [^{11}C] methionine pancreatic scanning with positron emission computed tomography. *J Nucl Med* 1979;20:778–781.

10. Syrota A, Collard P, Paraf A. Comparison of ^{11}C-L-methionine uptake by the parotid gland and pancreas in chronic pancreatitis studied by positron emission tomography. *Gut* 1983;24:637–641.
11. Syrota A, Dop-Ngassa M, Cerf M, Paraf A. ^{11}C-L-methionine for evaluation of pancreatic exocrine function. *Gut* 1981;22:907–915.
12. Brown M, Marshall DR, Sobel BE, et al. Delineation of myocardial oxygen utilization with carbon-11 labeled acetate. *Circulation* 1987;76:687–696.
13. Buxton DB, Nienaber CA, Luxen A, et al. Noninvasive quantitation of regional myocardial oxygen consumption in vivo with [1-^{11}C] acetate and dynamic positron emission tomography. *Circulation* 1989;79:134–142.
14. Armbrecht JJ, Buxton DB, Brunken RC, Phelps ME, Schelbert HR. Regional myocardial oxygen consumption determined noninvasively in humans with [1-^{11}C] acetate and dynamic positron emission tomography. *Circulation* 1989;80:863–872.
15. Beanlands RSB, Bach DS, Raylman R, et al. Acute effects of dobutamine on myocardial oxygen consumption and cardiac efficiency measured using carbon-11 acetate kinetics in patients with dilated cardiomyopathy. *J Am Coll Cardiol* 1993;22: 1389–1398.
16. Calderon P, Furnelle J, Christophe J. In vitro lipid metabolism in the rat pancreas I: basal lipid metabolism. *Biochim Biophys Acta* 1979;574:379–390.
17. Shreve PD, Chiao P-C, Humes HD, Schwaiger M, Gross MD. Carbon-11-acetate PET imaging in renal disease. *J Nucl Med* 1995;36:1595–1601.
18. Pike VW, Eakins MN, Allan RM, Selwyn AP. Preparation of [1-^{11}C] acetate: an agent for the study of myocardial metabolism by positron emission tomography. *Int J Appl Radiat Isot* 1982;33:505–512.
19. Rösch J. Roentgenologic diagnosis of pancreatic disease. *Am J Roentgenol* 1967;100: 664–672.
20. Gorelick FS, Jamieson JD. Structure-function relationships of the pancreas. In: Johnson LR, ed. *Physiology of the Gastrointestinal Tract.* New York: Raven Press; 1981:773–794.
21. Hansson E. The formation of pancreatic juice proteins studied with labelled amino acids. *Acta Physiol Scand* 1959;46(suppl 161):3–99.
22. Comar D, Cartron JC, Maziere M, et al. Labelling and metabolism of methionine-methyl-^{11}C. *Eur J Nucl Med* 1976;1:11–14.
23. Zuidema GD, Kirsh M, Turcotte JG, Gaisford JG, Powers W, Kowalczyk RS. Pancreatic uptake of Se^{75}-selenomethionine. *Ann Surg* 1963;158:894–897.
24. Braganza J, Critchley M, Howat HT, et al. An evaluation of ^{75}Se selenomethionine scanning as a test of pancreatic function compared with the secritin-pancreozymin test. *Gut* 1973;14:383–389.
25. Bares R, Klever P, Hauptmann S, et al. F-18 fluorodeoxyglucose PET *in vivo* evaluation of pancreatic glucose metabolism for detection of pancreatic cancer. *Radiology* 1994;192:79–86.
26. Kato T, Fukatsu H, Ito K, et al. Fluorodeoxyglucose positron emission tomography in pancreatic cancer: an unsolved problem. *Eur J Nucl Med* 1995;22:32–39.
27. Inokuma T, Tamaki N, Torizuka T, et al. Value of fluorine-18-fluorodeoxyglucose and thallium-201 in the detection of pancreatic cancer. *J Nucl Med* 1995;36:229–235.
28. Friess H, Langhans J, Ebert M, et al. Diagnosis of pancreatic cancer by 2[^{18}F]-fluoro-2-deoxy-D-glucose positron emission tomography. *Gut* 1995;36:771–777.
29. Inokuma T, Tamaki N, Torizuka T, et al. Evaluation of pancreatic tumors with positron emission tomography and F-18 fluorodeoxyglucose: comparison with CT and US. *Radiology* 1995;195:345–352. Population

Technetium-99m-Labeled Chemotactic Peptides in Acute Infection and Sterile Inflammation

Conny J. van der Laken, Otto C. Boerman, Wim J.G. Oyen, Marjo T.P. van de Ven, D. Scott Edwards, John A. Barrett, Jos W.M. van der Meer and Frans H.M. Corstens

Departments of Nuclear Medicine and Internal Medicine, University Hospital Nijmegen, Nijmegen, The Netherlands; and Radiopharmaceuticals Division, The Du Pont Merck Pharmaceutical Company, North Billerica, Massachusetts

Chemotactic peptides have been proposed as vehicles to image infection and inflammation. Previous studies have shown high uptake at the site of infection soon after injection, most likely because of specific binding to receptors on locally present leukocytes. To investigate this hypothesis, the in vivo behavior of a synthetic chemotactic peptide was compared to a control peptide of similar molecular weight with low receptor binding affinity. In addition, the potential to target to different infections and sterile inflammation was tested. **Methods:** Twenty-four hours after induction of *Escherichia coli*, *Staphylococcus aureus* and zymosan abscesses, rabbits were i.v. injected with either 1 mCi of ^{99m}Tc-labeled formyl-methionyl-leucyl-phenylalanyl-lysine-hydrazinonicotinamide (^{99m}Tc-fMLFK-HYNIC) or ^{99m}Tc-labeled hydrazinonicotinamide-methionyl-leucyl-phenylalanyl-OMe (^{99m}Tc-HYNIC-MLFOMe, control peptide). Gamma camera images were obtained at 5 min and 1, 4, 8 and 20 hr postinjection. Biodistribution was determined at 20 hr postinjection. **Results:** The blood clearances of ^{99m}Tc-fMLFK-HYNIC and ^{99m}Tc-HYNIC-MLFOMe were similar. With time, ^{99m}Tc-fMLFK-HYNIC was retained in the abscess (*E. coli*), whereas the control agent ^{99m}Tc-HYNIC-MLFOMe was cleared from the abscess (0.049 ± 0.011 versus 0.005 ± 0.0003%ID/g at 20 hr postinjection; $p < 0.0005$). Abscess-to-contralateral muscle ratios of ^{99m}Tc-fMLFK-HYNIC rose to 36.8 ± 4.3 at 20 hr postinjection. *E. coli*, *S. aureus* and zymosan abscesses were clearly visualized from 4 hr postinjection onward. Abscess-to-background ratios increased to values varying from 4.4 ± 0.2 (zymosan) to 7.1 ± 0.6 (*S. aureus*) at 20 hr postinjection. The uptake in *S. aureus* and zymosan abscesses did not differ significantly from the uptake in *E. coli* abscesses. **Conclusion:** fMLFK-HYNIC is retained in both acute infection and sterile inflammation by means of specific receptor binding if sufficient cellular infiltration is present.

Key Words: chemotactic peptides; infection; inflammation; biodistribution; imaging

J Nucl Med 1997; 38:1310–1315

During the past few years, there has been a growing interest in the development of radiolabeled immunopeptides and proteins as radiopharmaceuticals for the imaging of infection and inflammation. Their small size and receptor binding capacity may make radiolabeled immunopeptides suitable agents for the rapid detection of inflammatory foci. The potential of several immunopeptides and proteins has already been demonstrated (*1–5*). One promising approach is the use of chemotactic peptides (*6*).

Chemotactic peptides, released by bacteria, cause leukocytes to marginate to nearby endothelial surfaces, move extravascularly and accumulate at sites where a chemotactin has been generated, a process called chemotaxis (*7*). Migration of cells from the blood to sites of tissue damage in the extravascular tissue is crucial to the development of inflammation. Schiffmann et al. (*8*) found that formyl peptides, synthetic analogs of natural bacterial products, were potent chemotactic factors for polymorphonuclear neutrophils (PMNs) and monocytes. These peptides initiate leukocyte chemotaxis by high-affinity binding to receptors present on both PMNs and mononuclear cells (*9,10*).

Fischman et al. (*1*) and Babich et al. (*2*) showed that acute infection in rats, rabbits and nonhuman primates can be clearly

Received Oct. 4, 1996; revision accepted Feb. 19, 1997.

For correspondence or reprints contact: Conny J. van der Laken, MD, Department of Nuclear Medicine, University Hospital Nijmegen, P.O. Box 9101, 6500 HB Nijmegen, The Netherlands.